Monte Carlo simulations of liquid crystals between microstructured substrates

Monte Carlo simulations of liquid crystals between nanostructured substrates

David L. Cheung*†

Department of Physics and Centre for Scientific Computing, University of Warwick, Coventry, CV4 7AL, UK

Abstract

The structure of a model liquid crystalline fluid, confined between two nanostructured substrates is studied through Monte Carlo simulations. A simple model for a structured substrate, similar in spirit to those used for rough walls or walls with grafted polymers, is introduced. It is found that varying the structure of the substrate a transition in the alignment of the confined fluid, from parallel to perpendicular, is induced. For particular substrate structures it is possible to induced tilted alignment in the confined fluid, the tilt angle being temperature dependent.

PACS numbers: 61.30Hn, 61.30Cz, 68.08-p

* Present address: Department of Chemistry, University of Warwick, Coventry, CV4 7AL,UK
†Electronic address: david.cheung@warwick.ac.uk

I. INTRODUCTION

The behavior of liquid crystals in the vicinity of solid substrates is both scientifically interesting and important in many of their applications [1]. The alignment of the nematic director along a given direction with respect to the surface, a phenomena termed surface-anchoring, is important in displays and other optoelectronic devices. This is particularly true for recently developed bistable LC devices [2–4]. Despite this importance, the physical mechanisms that control the direction and strength of this anchoring are still poorly understood.

Due to the importance of interactions between LCs and solid substrates there have been a large number of studies performed with molecular simulations [5–10], and theories such as density functional theory (DFT) [8, 11–13]. These have largely concentrated an simple homogeneous surfaces and has investigated phenomena such as surface anchoring strength [8, 9] and capillary nematization [14, 15].Recently there have been a number of studies that have investigated the effect of changes in the surface structure on LC. Rod-shaped LCs near grooved surfaces show unusual smectic-C ordering in the vicinity of the surface [16]. More recently the anchoring strength and surface tension for LCs near grooved surfaces have been calculated from molecular dynamics simulations [17]. The structure of a hard-rod fluid, modelled using the Zwanzig model, near square-grooved surfaces have been studied using DFT [18]. Monte Carlo (MC) simulations of LCs confined by rough surfaces have shown a decrease in anchoring strength [19] and a shift in the isotropic-nematic transition pressure [20] with increasing surface roughness. Simulations of LCs near surfaces with grafted polymer brushes, using both single-site [21–24] and atomistic [25] models have shown anchoring transitions with increasing polymer grafting density. Anchoring transitions on flat, planar surfaces can also be triggered through changes in the LC-surface interaction [26, 27].

In this paper a model liquid crystal thin film, confined between two structured substrates is studied. The substrate consists of a smooth planar wall, with a regular array of interaction sites embedded in them. By choosing competing interactions, i.e. planar (parallel) alignment at the bare wall and end-on interaction between fluid molecules and embedded atoms, an anchoring transition may be induced. Such a transition may be driven by either changes in surface structure (e.g. density of embedded atoms) or by changing thermodynamic quantities. Previous studies, such as those on polymer grafted surfaces [21–24], have

employed purely repulsive (athermal) interactions so the anchoring transitions were entropically driven. By incorporating attractive terms into the intermolecular and molecule-wall interactions, as detailed in the following section, the effect of temperature may be investigated.

II. MODEL AND SIMULATION DETAILS

The fluid molecules interact through the well-known Gay-Berne potential [28]. For two molecules with positions $\boldsymbol{r}_i$ and $\boldsymbol{r}_j$, and orientations $\boldsymbol{u}_i$ and $\boldsymbol{u}_j$, the interaction potential is given by

$$V_{GB}(\boldsymbol{r}_{ij}, \boldsymbol{u}_i, \boldsymbol{u}_j) = 4\epsilon_{GB}(\hat{\boldsymbol{r}}_{ij}, \boldsymbol{u}_i, \boldsymbol{u}_j) \left[\left(\frac{\sigma_0}{r - \sigma(\hat{\boldsymbol{r}}_{ij}, \boldsymbol{u}_i, \boldsymbol{u}_j) + \sigma_0} \right)^{12} - \left(\frac{\sigma_0}{r - \sigma(\hat{\boldsymbol{r}}_{ij}, \boldsymbol{u}_i, \boldsymbol{u}_j) + \sigma_0} \right)^{6} \right] \tag{1}$$

where $\boldsymbol{r}_{ij} = \boldsymbol{r}_i - \boldsymbol{r}_j$, $r = |\boldsymbol{r}|$ and $\hat{r} = \boldsymbol{r}/r$. The orientationally dependent width is given by

$$\sigma(\boldsymbol{r}_{ij}, \boldsymbol{u}_i, \boldsymbol{u}_j) = \sigma_0 \left[1 - \frac{\chi}{2} \left(\frac{(\hat{\boldsymbol{r}}_{ij}.\boldsymbol{u}_i + \hat{\boldsymbol{r}}_{ij}.\boldsymbol{u}_j)^2}{1 + \chi \boldsymbol{u}_i.\boldsymbol{u}_j} + \frac{(\hat{\boldsymbol{r}}_{ij}.\boldsymbol{u}_i - \hat{\boldsymbol{r}}_{ij}.\boldsymbol{u}_j)^2}{1 - \chi \boldsymbol{u}_i.\boldsymbol{u}_j} \right) \right]. \tag{2}$$

where $\chi = (1 - \kappa^2)/(1 + \kappa^2)$ and the energy parameter is

$$\epsilon_{GB}(\boldsymbol{r}_{ij}, \boldsymbol{u}_i, \boldsymbol{u}_j) = \epsilon_0 \epsilon_{GB} \left(\boldsymbol{u}_i.\boldsymbol{u}_j \right)^{\nu} \epsilon'_{GB} \left(\boldsymbol{U}_i, \boldsymbol{u}_j, \boldsymbol{r}_{ij} \right)^{\mu} \tag{3}$$

where

$$\epsilon_{GB} \left(\boldsymbol{u}_i.\boldsymbol{u}_j \right) = \left[1 - \chi^2 \left(\boldsymbol{u}_i.\boldsymbol{u}_j \right)^2 \right]^{\frac{1}{2}} \tag{4}$$

and

$$\epsilon'_{GB} \left(\boldsymbol{u}_i, \boldsymbol{u}_j, \boldsymbol{r}_{ij} \right) = \left[1 - \frac{\chi'}{2} \left(\frac{(\hat{\boldsymbol{r}}_{ij}.\boldsymbol{u}_i + \hat{\boldsymbol{r}}_{ij}.\boldsymbol{u}_j)^2}{1 + \chi' \boldsymbol{u}_i.\boldsymbol{u}_j} + \frac{(\hat{\boldsymbol{r}}_{ij}.\boldsymbol{u}_i - \hat{\boldsymbol{r}}_{ij}.\boldsymbol{u}_j)^2}{1 - \chi' \boldsymbol{u}_i.\boldsymbol{u}_j} \right) \right] \tag{5}$$

with $\chi' = (1 - \kappa'^{1/\mu})/(1 + \kappa'^{1/\mu})$. The Gay-Berne model contains four adjustable parameters, κ, κ', μ, and ν. In this work the frequently used values of $\kappa = 3$, $\kappa' = 5$, $\mu = 2$, and $\nu = 1$ for which the bulk phase behavior has been well studied [29, 30] are adopted. The GB width σ_0 and energy ϵ_0 parameters are used to define reduced units throughout this work, with the reduced density $\rho^* = \rho \sigma_0^{-3}$ and temperature $T^* = k_B T/\epsilon_0$.

The fluid-wall interaction consists of two parts. The first is a repulsive LJ interaction given by

$$V_W(\boldsymbol{r}_i, \boldsymbol{u}_i) = \begin{cases} 4\left[\left(\frac{\sigma_0}{z_i - \sigma_w(\boldsymbol{u}_i) + \sigma_0}\right)^{12} - \left(\frac{\sigma_0}{z_i - \sigma_w(\boldsymbol{u}_i) + \sigma_0}\right)^{6}\right], & z_i - \sigma_w(\boldsymbol{u}_i) < 2^{1/6} \\ 0 & , \; z_i - \sigma_w(\boldsymbol{u}_i) > 2^{1/6} \end{cases} \tag{6}$$

where

$$\sigma_w(\boldsymbol{u}_i) = \frac{1}{2}\sqrt{1 + (\kappa_w^2 - 1)u_{iz}^2}. \tag{7}$$

In this work $\kappa_w = 3$, which gives rise to planar alignment at the substrate [21]. Structure is introduced into the substrate by embedding a regular square array of spherical interaction sites in the wall. These interact with the fluid molecules through a generalization of Eq. 1 [31, 32], with the shape parameter given by

$$\sigma_{rs}(\boldsymbol{r}_{ij}, \boldsymbol{u}_i) = \sigma_0 \left[1 - \chi(\hat{\boldsymbol{r}}_{ij}.\boldsymbol{u}_i)^2\right]^{-1/2} \tag{8}$$

and the energy parameter

$$\epsilon_{rs} = \epsilon_{rs}^0 \left[1 - \left(1 - \left(\frac{\epsilon_e}{\epsilon_s}\right)^{1/\mu}\right)(\hat{\boldsymbol{r}}_{ij}.\boldsymbol{u}_i)^2\right]^{\mu} \tag{9}$$

where $\epsilon_{rs}^0 = 1$, $\mu = 2$ and the ratio ϵ_e/ϵ_s controls the side-to-end well depth anisotropy. In this work $\epsilon_e/\epsilon_s = \kappa' = 5$. Simulations of GB-LJ mixtures using this potential have shown that the LJ sites favor the ends of the GB molecules for this set of parameters [32].

The systems studied consisted of 1080 GB molecules in a cubic box of side length $15\sigma_0$, giving an overall density $\rho^* = 0.32$ (although due to the excluded volume of the walls, the volume accessible to the fluid molecules in somewhat lower, and the density is correspondingly larger ($\rho^* = 0.342$)). Simulations were performed for a range of reduced temperatures $T^* = 0.90, 1.00, 1.05, 1.10, 1.15, 1.20$. To check for system size effects a few simulations were performed on systems of 2160 molecules with a box length of $30\sigma_0$ in the z-direction (wall normal). Surfaces with 2×2, 3×3, 4×4, 5×5 and 8×8 arrays were studied (separation between atomic sites of $7.5\sigma_0$, $5.0\sigma_0$, $3.75\sigma_0$, $3.0\sigma_0$ and $1.75\sigma_0$). The requirement of the array to be commensurate with the periodic boundaries in the x and y directions limits the values of atomic separation that may be studied. Shown in Fig. 1 are maps of the potential for representative surfaces. A spherical cut-off of $r_{\rm cut} = 4.0\sigma_0$ applied to interactions between the fluid molecules and between fluid molecules and wall atoms. For each reduced temperature and surface density approximately 1 million MC sweeps (1 attempted translation and 1

attempted rotation per molecule) were used for equilibration, then statistics were gathered over a further 1 million sweeps.

The distribution of molecules in the simulation cell may be described by the density profile $\rho(z)$. To describe the ordering through the cell, the ordering tensor can be calculated throughout the cell. This is given by

$$Q_{\alpha\beta}(z) = \left\langle \frac{3}{2} u_{i\alpha} u_{i\beta} - \frac{1}{2}\delta_{\alpha\beta} \right\rangle_z \tag{10}$$

where $\alpha, \beta = x, y, z$ and $\delta_{\alpha\beta}$ is the Kronecker delta. The angled brackets denote an average over all molecules in the region $z - 0.5\delta z$ to $z + 0.5\delta z$. Diagonalising this gives the order parameter profiles ($q_+(z)$, $q_0(z)$, and $q_-(z)$). These can be expressed as $S(z)$, $S(z)+\frac{1}{2}S_{xy}(z)$, and $S(z) - \frac{1}{2}S_{xy}(z)$, where $S(z)$ is the nematic order parameter and $S_{xy}(z)$ is the biaxiality parameter. The nematic director $\mathbf{n}(z)$ can be identified with the eigenvector of the ordering tensor corresponding to the largest eigenvalue. Particularly important is the director tilt angle (with respect to the surface normal), given by $\theta(z) = \cos^{-1}(n_z(z))$.

III. RESULTS

Shown in Fig. 2 are the density, order parameter, biaxiality and director tilt angle profiles for the confined GB film at a reduced temperature of $T^* = 1.20$. For the smooth surface the structure of the fluid is similar to that seen in previous works [6, 23, 33]. There is a peak in $\rho(z)$ at $z \approx 0.5\sigma_0$ and layers with periodicity $\approx 1\sigma_0$ decaying into the cell bulk. Similar structure appears in the order parameter profile, while there is a peak in the biaxiality profile near the surface. Biaxiality near hard (in the sense of excluding the entire molecule) walls has been observed for hard core fluids [14, 24, 34]. The profiles for the 2×2 wall (not shown) are very close to those of the smooth wall.

For the 3×3 surface there is a decrease in the density and increase in the biaxiality in the vicinity of the surface. The surface atoms have a larger effect on the order parameter profile, with a decrease in the order parameter around the density peak and a region of reduced order decaying into the bulk. For higher densities the embedded atoms have a more dramatic effect on the structure of the confined fluid. Due to the increased attraction between the fluid and the surface, a layer structure, indicated by periodic variations in $\rho(z)$, appears. As the number of embedded atoms increases this layering becomes more pronounced. In addition

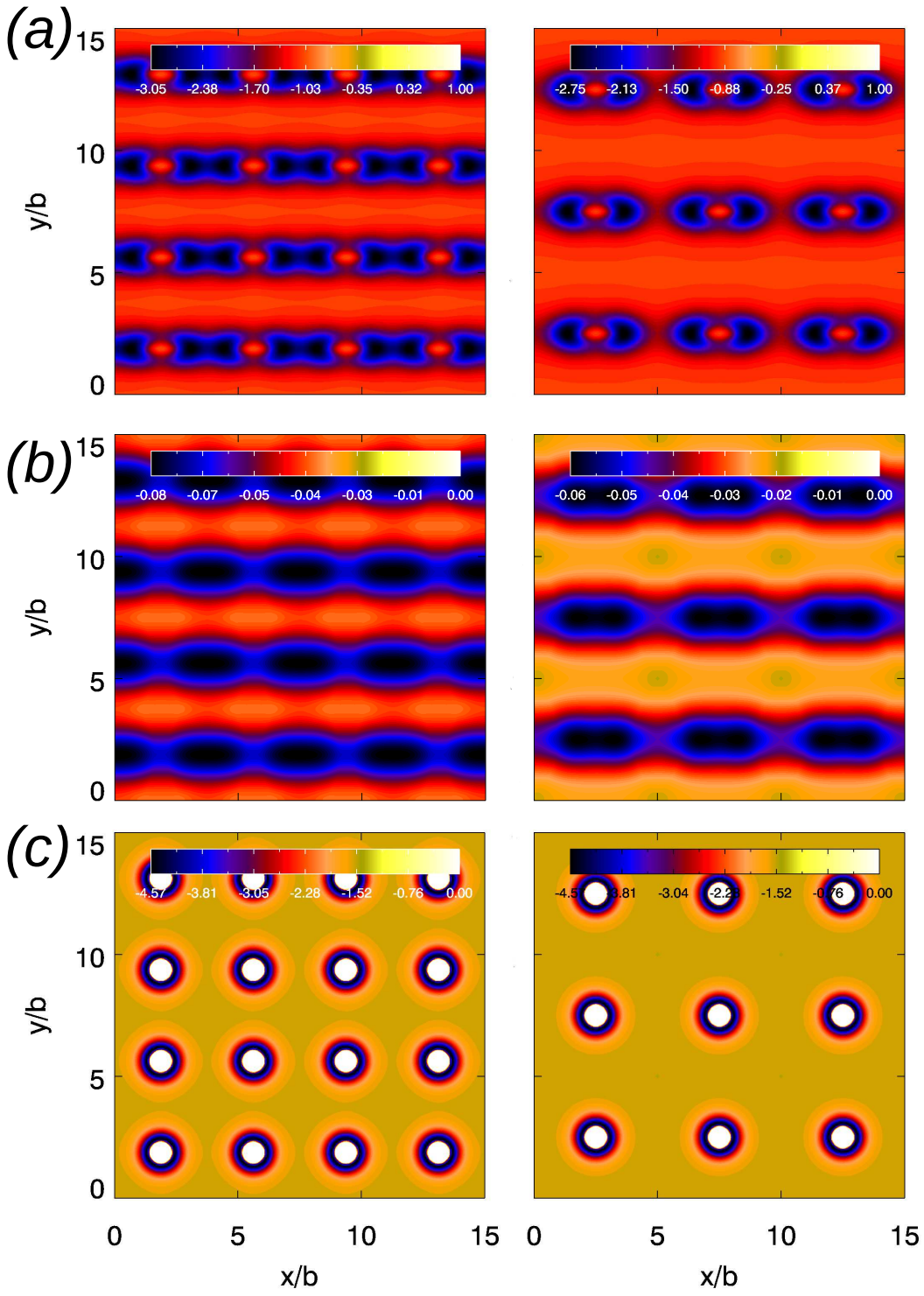

FIG. 1: (Color online) Contour maps of potential energy surface for (a) $z = 1\sigma_0$ and $\boldsymbol{u} = (1, 0, 0)$, (b) $z = 2\sigma_0$ and $\boldsymbol{u} = (1, 0, 0)$ and (c) $z = 2\sigma_0$, $\boldsymbol{u} = (0, 0, 1)$.Left hand column shows maps for 4×4 surface, right hand side 3×3 surface.

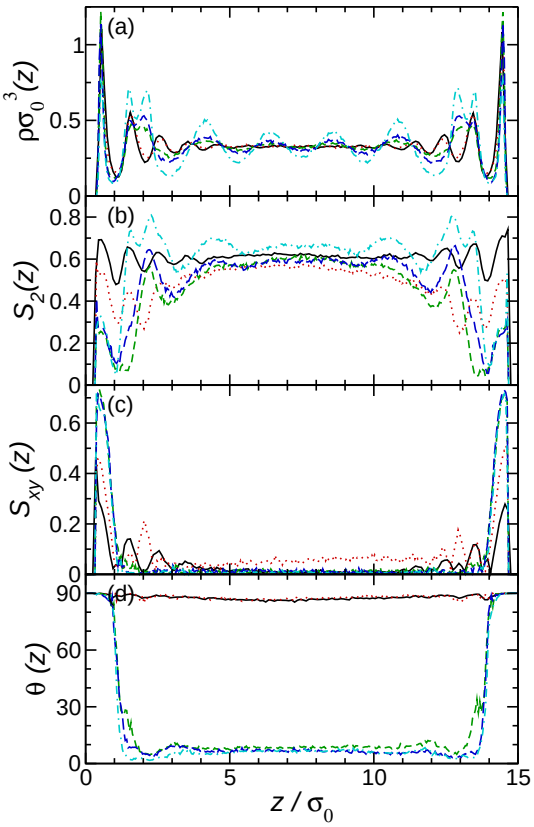

FIG. 2: (Color online) (a) Density, (b) order parameter, (c) biaxiality, and (d) director tilt angle profiles for GB fluid at reduced temperature $T^* = 1.20$. Data for smooth surface shown by solid line, 3×3 surface dotted line, 4×4 surface dashed line, 5×5 surface long-dashed line, and 8×8 surface dot-dashed line (online: black, red, green, blue, and cyan respectively).

the second peak in the density profile becomes broader then splits into two as the number of surface atoms increases. This suggests that the first layer of molecules acts as a rough wall for the remainder of the fluid [15]. In the vicinity of the surface there is a marked decrease in the order parameter and increase in the biaxiality. The director tilt angle profile (Fig. 2(d)) shows an abrupt change from planar anchoring at the surface to homeotropic anchoring in the cell bulk, caused by the preference of end-on interactions between the GB molecules and wall atoms. Such abrupt changes in alignment have been observed in simulations of GB molecules adsorbed on graphite surfaces [35].

More insight into the structure of the confined fluid may be gained by examination of simulation snapshots (Fig. 3). Side on views of the simulation cell clearly show the change in alignment caused by the change in surface structure. By viewing the layer of molecules

adsorbed on the surface, the differences for different surface may be clearly seen. For the smooth surface this layer is aligned along a single direction. Snapshots for the patterned surfaces show the tendency of the molecules to align end-on to the surface atoms. It is noticeable that for the 3×3 array molecules near the surface may only interact with a single surface atom (the interatomic spacing is significantly larger than the molecular length), while for the other surfaces fluid molecules may interaction with two or more surface atoms. For the 4×4 and 5×5 arrays, where the spacing between the atoms is slightly larger than the molecular length the molecules lie on the surface, so as to maximize the attractive interaction (molecules lying either along the x and y axes for the 4×4 array or at 45° for the 5×5 array). This gives rise to the peak in $S_{xy}(z)$ seen in Fig. 2 and the decrease in the order parameter in the vicinity of the surface. For the 8×8 array, where the atomic spacing is smaller than the molecular length, the fluid molecules have lie on top of the surface atoms.

The location of the anchoring transition at atomic spacings comparable to the molecular length deserves some comment. When the separation between the surface atoms is commensurate with the molecular length the strong preference for molecules to lie between two surface atoms leads to noticable gaps in the distribution of molecules at the surface (e.g. Fig. 3(c)). These gaps allow molecules in the second layer from the surface are then able to lie end on to the surface; the molecule-surface energy for normal alignment is significantly lower then for parallel alignment for molecules $z \approx 1.5 - 2\sigma_0$ (Fig. 1).By contrast the distribution of molecules on the 3×3 surface (Fig. 3(b)) is more homogeneous, so molecules in the second layer lie parallel to the molecules adsorbed on the surface.

The effect of changing temperature on the structure can be seen in Figs. 4 and 5. For the smooth wall, on decreasing T^* the confined fluid becomes more strongly structured, with a stronger layering seen in the density profile and the order parameter in the centre of the cell increasing. The 3×3 array shows the most dramatic variation with temperature. On decreasing T the director in the cell bulk changes from parallel alignment to tilted ($\theta \approx 20^\circ$) at $T^* = 1.00$ to close to normal ($\theta \approx 10^\circ$) at $T^* = 0.90$. The peak in $S_{xy}(z)$ near the wall increases to ≈ 0.80, comparable to the denser substrates. For the denser surfaces the no comparably dramatic changes in the profiles are observed; the layering seen in the density profile becomes stronger and the order parameter in the cell bulk increasing with decreasing temperature.

The effect of changing surface coverage and temperature on the director tilt angle in the

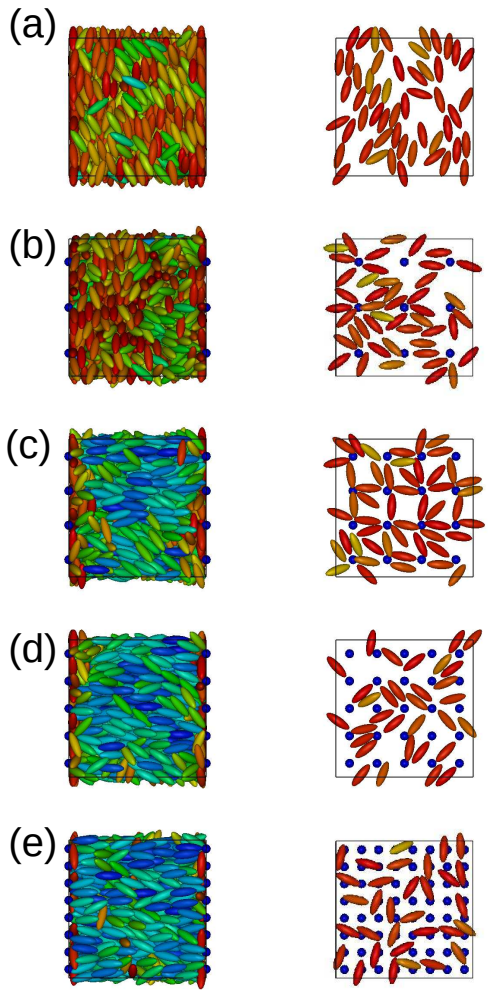

FIG. 3: (Color online) Simulation snapshots for confined GB at $T^* = 1.20$ for (a) smooth surface, (b) 3×3 array, (c) 5×5 array, and (d) 8×8 array. Left hand column shows side view, right hand column shows molecules within $1\sigma_0$ of surface (online: molecules color-coded according to orientation). Spheres (online: blue) show position of surface atoms. Snapshots generated using the QMGA package [36].

cell bulk (the central $l_z/2$ of the cell) is shown in Fig. 6(a). $\theta \approx 90°$ at all temperatures for the smooth wall. θ_0 for 2×2 surface similar shows little variation with T, remaining close to $90°$ for all T^*. For the 4×4-8×8 surfaces there is only a slight change in the tilt angle: for the 8×8 surface θ drops from $\approx 7°$ ($T^* = 1.20$) to $\approx 5°$ ($T^* = 0.90$). The 3×3 array shows the most variation with with temperature with $\theta_0 \approx 80°$ at high temperatures ($T^* > 1.1$) and $\theta^* < 20°$ at low temperatures ($T^* < 0.90$). For a small temperature range the director adopts a tilted alignment. Figure 6 (b) shows the director tilt angle profiles for the 3×3

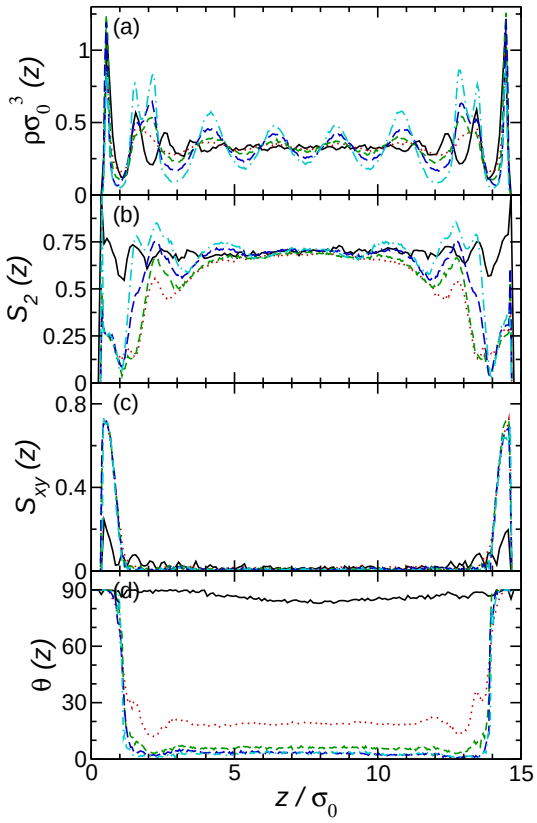

FIG. 4: (Color online) (a) Density, (b) order parameter, (c) biaxiality, and (d) director tilt angle profiles for GB fluid at reduced temperature $T^* = 1.00$. Data for smooth surface shown by solid line, 3×3 surface dotted line, 4×4 surface dashed line, 5×5 surface long-dashed line, and 8×8 surface dot-dashed line (online: black, red, green, blue, and cyan respectively).

surface for all the temperatures studied. At all temperatures the tilt angle is constant in the cell bulk. The director twist angle also shows little variation in the cell bulk (not shown), so the changes in the surface structure promote roughly uniform alignment.

IV. CONCLUSIONS

The structure of a confined thin film of a model liquid crystal has been studied using Monte Carlo simulations. Structure is introduced into the substrates by embedding a regular array of spherical interaction sites, in similar manner to recent studies of LCs on rough surfaces [19, 20]. The interactions between the fluid molecules and these interaction sites are chosen to be in competition with the bare wall potential. On increasing the density of these embedded atoms a transition from parallel to normal alignment is seen. When

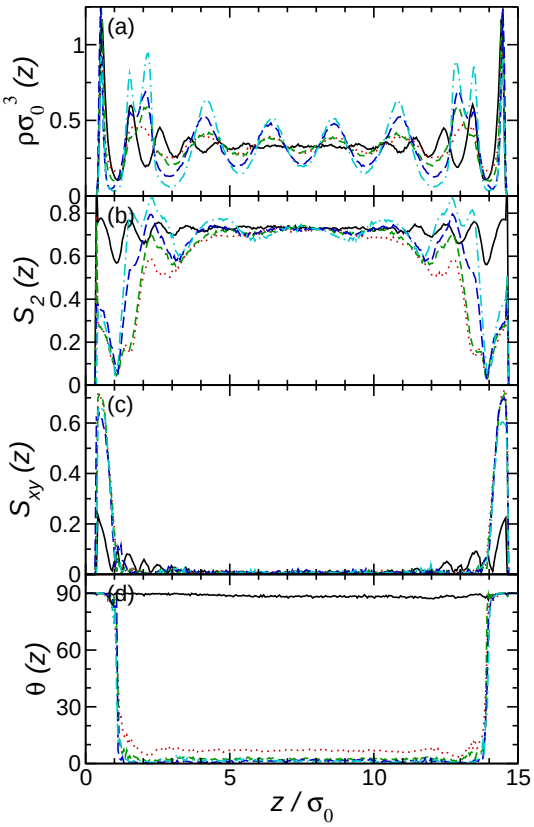

FIG. 5: (Color online) (a) Density, (b) order parameter, (c) biaxiality, and (d) director tilt angle profiles for GB fluid at reduced temperature $T^* = 0.90$. Data for smooth surface shown by solid line, 3×3 surface dotted line, 4×4 surface dashed line, 5×5 surface long-dashed line, and 8×8 surface dot-dashed line (online: black, red, green, blue, and cyan respectively).

the separation between the surface atoms is comparable to or shorter than the molecular length, the alignment is normal throughout the nematic range, due to thestrong attraction between the molecule ends and the surface. For intermediate separations the alignment at high temperatures is parallel to the surface, commensurate with the bare wall. When the temperature is decreased alignment changes first to tilted then to normal. This temperature dependence may be understood as the attractive interation between the molecule ends and the wall atoms becomes increasingly importantat lower T. The temperature dependence of the tilt is in contrast to previous studies [24] that employed purely repulsive interactions. In these studies the anchoring transitions are driven solely by entropy. In the present model the transition is driven by the interplay between the attraction between the surface atoms and fluid molecules (which would give rise to normal alignment) and the excluded volume

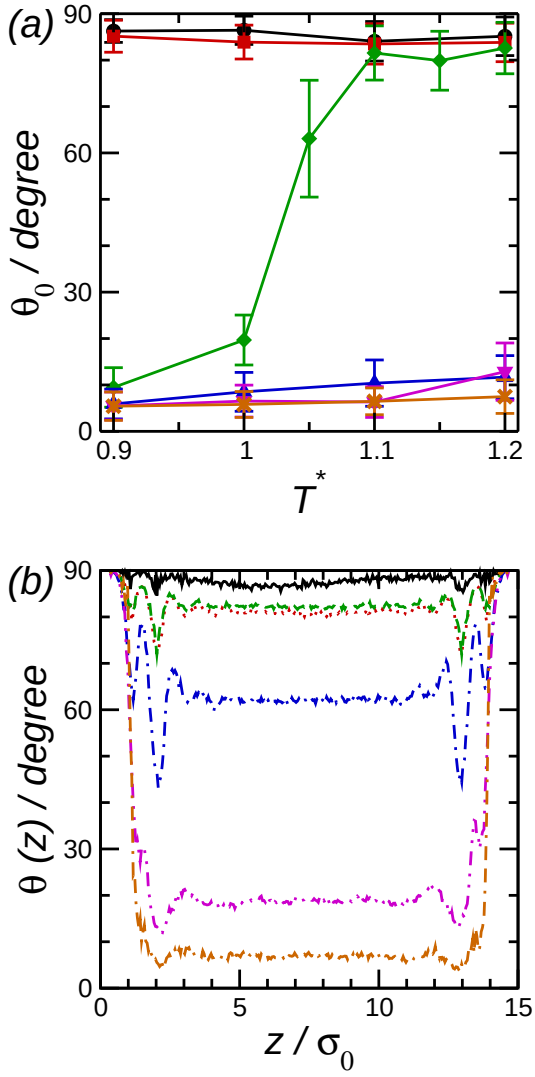

FIG. 6: (Color online)(a) Director tilt angle against temperature for smooth substrate (circles, online: black), 2×2 array (squares, online: red), 3×3 array (diamonds, online: green) and 4×4 array (triangles, online: blue), 5×5 array (inverted triangles, online: magenta), and 8×8 array (crosses, online: orange). (b) Director angle profiles for the 3×3 array at $T^* = 1.20$ (solid line, black), $T^* = 1.15$ (dotted line, red), $T^* = 1.10$ (dashed line, green), $T^* = 1.05$ (dot-dashed line, blue), $T^* = 1.00$ (double-dot-dashed line, magenta), and $T^* = 0.90$ (dot-double-dashed line, orange).

effect of the surface (which would give rise to parallel alignment).

Acknowledgements

The author is grateful to Prof. Mike Allen for helpful advice and a critical reading of this manuscript. This research was supported by EPSRC grant GR/S77240. The calculations were performed on the computing facilities of the Centre for Scientific Computing, University of Warwick.

---

[1] B. Jérôme, Rep. Prog. Phys. **54**, 391 (1991).

[2] G. P. Bryan-Brown, C. V. Brown, I. C. Sage, and V. C. Hui, Nature **392**, 365 (1998).

[3] A. J. Davidson and N. J. Mottram, Phys. Rev. E **65**, 051710/1 (2002).

[4] C. Denniston and J. M. Yeomans, Phys. Rev. Lett. **87**, 27505/1 (2002).

[5] T. Gruhn and M. Schoen, Phys. Rev. E **55**, 2861 (1997).

[6] G. D. Wall and D. J. Cleaver, Phys. Rev. E **56**, 4306 (1997).

[7] H. Steuer, S. Hess, and M. Schoen, Phys. Rev. E **69**, 031708/1 (2004).

[8] M. P. Allen, Molec. Phys. **96**, 1391 (1999).

[9] D. Andrienko, G. Germano, and M. P. Allen, Phys. Rev. E **62**, 6688 (2000).

[10] Z. Zhang, A. Chakrabarti, O. G. Mouritsen, and M. J. Zuckermann, Phys. Rev. E **53**, 2461 (1996).

[11] H. de las Heras, L. Mederos, and E. Velasco, Phys. Rev. E **68**, 031709/1 (2003).

[12] D. L. Cheung and F. Schmid, J. Chem. Phys. **120**, 9185 (2004).

[13] A. Chrzanowska, P. I. C. Teixeira, H. Ehrentraut, and D. J. Cleaver, J. Phys. Cond. Mat. **13**, 4715 (2001).

[14] M. Dijkstra, R. van Roij, and R. Evans, Phys. Rev. E **63**, 051703 (2001).

[15] M. M. Piñeiro, A. Galindo, and A. O. Parry, Soft Matter **3**, 768 (2007).

[16] J. Stelzer, P. Galatola, G. Barbero, and L. Longa, Phys. Rev. E **55**, 477 (1997).

[17] K. Kiyohara, K. Asaka, H. Monobe, N. Terasawa, and Y. Shimizu, J. Chem. Phys. **124**, 034704/1 (2006).

[18] L. Harnau, F. Penna, and S. Dietrich, Phys. Rev. E **70**, 021505/1 (2004).

[19] D. L. Cheung and F. Schmid, J. Chem. Phys. **122**, 074902/1 (2005).

[20] D. L. Cheung and F. Schmid, Chem. Phys. Lett. **418**, 392 (2006).

[21] H. Lange and F. Schmid, Euro. Phys. J. E **7**, 175 (2002).

[22] H. Lange and F. Schmid, Comput. Phys. Commun. **147**, 276 (2002).

[23] H. Lange and F. Schmid, J. Chem. Phys. **117**, 362 (2002).

[24] M. T. Downton and M. P. Allen, Europhys. Lett. **65** (2004).

[25] M. T. Downton and S. Hanna, Europhys. Lett. **74**, 69 (2006).

[26] F. Barmes and D. J. Cleaver, Phys. Rev. E **69**, 061705/1 (2004).

[27] F. Barmes and D. J. Cleaver, Phys. Rev. E **71**, 021705/1 (2005).

[28] J. G. Gay and B. J. Berne, J. Chem. Phys. **74**, 3316 (1981).

[29] E. de Miguel, L. F. Rull, M. K. Chalam, and K. E. Gubbins, Molec. Phys. **74**, 405 (1991).

[30] E. De Miguel, Molec. Phys. **100**, 2449 (2002).

[31] B. J. Berne and P. Pechukas, J. Chem. Phys. **56**, 4213 (1972).

[32] D. Antypov and D. J. Cleaver, J. Chem. Phys. **120**, 10307 (2004).

[33] P. I. C. Teixeira, F. Barmes, and D. J. Cleaver, J. Phys. Cond. Mat. **16**, S1969 (2004).

[34] A. Poniewierski, Phys. Rev. E **47**, 3396 (1993).

[35] V. Palermo and C. Biscarini, F. Zannoni, Phys. Rev. E **57**, R2519 (1998).

[36] A. T. Gabriel, T. Meyer, and G. Germano, J. Chem. Theory Comput. **4**, 468 (2008), URL `http://qmga.sourceforge.net`.

Figure Captions

Fig. 1. (Color online) Contour maps of potential energy surface for (a) $z = 1\sigma_0$ and $\boldsymbol{u} = (1, 0, 0)$, (b) $z = 2\sigma_0$ and $\boldsymbol{u} = (1, 0, 0)$ and (c) $z = 2\sigma_0$, $\boldsymbol{u} = (0, 0, 1)$. Left hand column shows maps for 4×4 surface, right hand side 3×3 surface.

Fig. 2. (Color online) (a) Density, (b) order parameter, (c) biaxiality, and (d) director tilt angle profiles for GB fluid at reduced temperature $T^* = 1.20$. Data for smooth surface shown by solid line, 3×3 surface dotted line, 4×4 surface dashed line, 5×5 surface long-dashed line, and 8×8 surface dot-dashed line (online: black, red, green, blue, and cyan respectively).

Fig. 3. (Color online) Simulation snapshots for confined GB at $T^* = 1.20$ for (a) smooth surface, (b) 3×3 array, (c) 5×5 array, and (d) 8×8 array. Left hand column shows side view, right hand column shows molecules within $1\sigma_0$ of surface (online: molecules color-coded according to orientation). Spheres (online: blue) show position of surface atoms. Snapshots generated using the QMGA package [36].

Fig. 4. (Color online) (a) Density, (b) order parameter, (c) biaxiality, and (d) director tilt angle profiles for GB fluid at reduced temperature $T^* = 1.00$. Data for smooth surface shown by solid line, 3×3 surface dotted line, 4×4 surface dashed line, 5×5 surface long-dashed line, and 8×8 surface dot-dashed line (online: black, red, green, blue, and cyan respectively).

Fig. 5. (Color online) (a) Density, (b) order parameter, (c) biaxiality, and (d) director tilt angle profiles for GB fluid at reduced temperature $T^* = 0.90$. Data for smooth surface shown by solid line, 3×3 surface dotted line, 4×4 surface dashed line, 5×5 surface long-dashed line, and 8×8 surface dot-dashed line (online: black, red, green, blue, and cyan respectively).

Fig. 6. (Color online)(a) Director tilt angle against temperature for smooth substrate (circles, online: black), 2×2 array (squares, online: red), 3×3 array (diamonds, online: green) and 4×4 array (triangles, online: blue), 5×5 array (inverted triangles, online: magenta), and 8×8 array (crosses, online: orange). (b) Director angle profiles for the 3×3 array at $T^* = 1.20$ (solid line, black), $T^* = 1.15$ (dotted line, red), $T^* = 1.10$

(dashed line, green), $T^* = 1.05$ (dot-dashed line, blue), $T^* = 1.00$ (double-dot-dashed line, magenta), and $T^* = 0.90$ (dot-double-dashed line, orange).

Fig. 1 D. L. Cheung

Journal of Chemical Physics

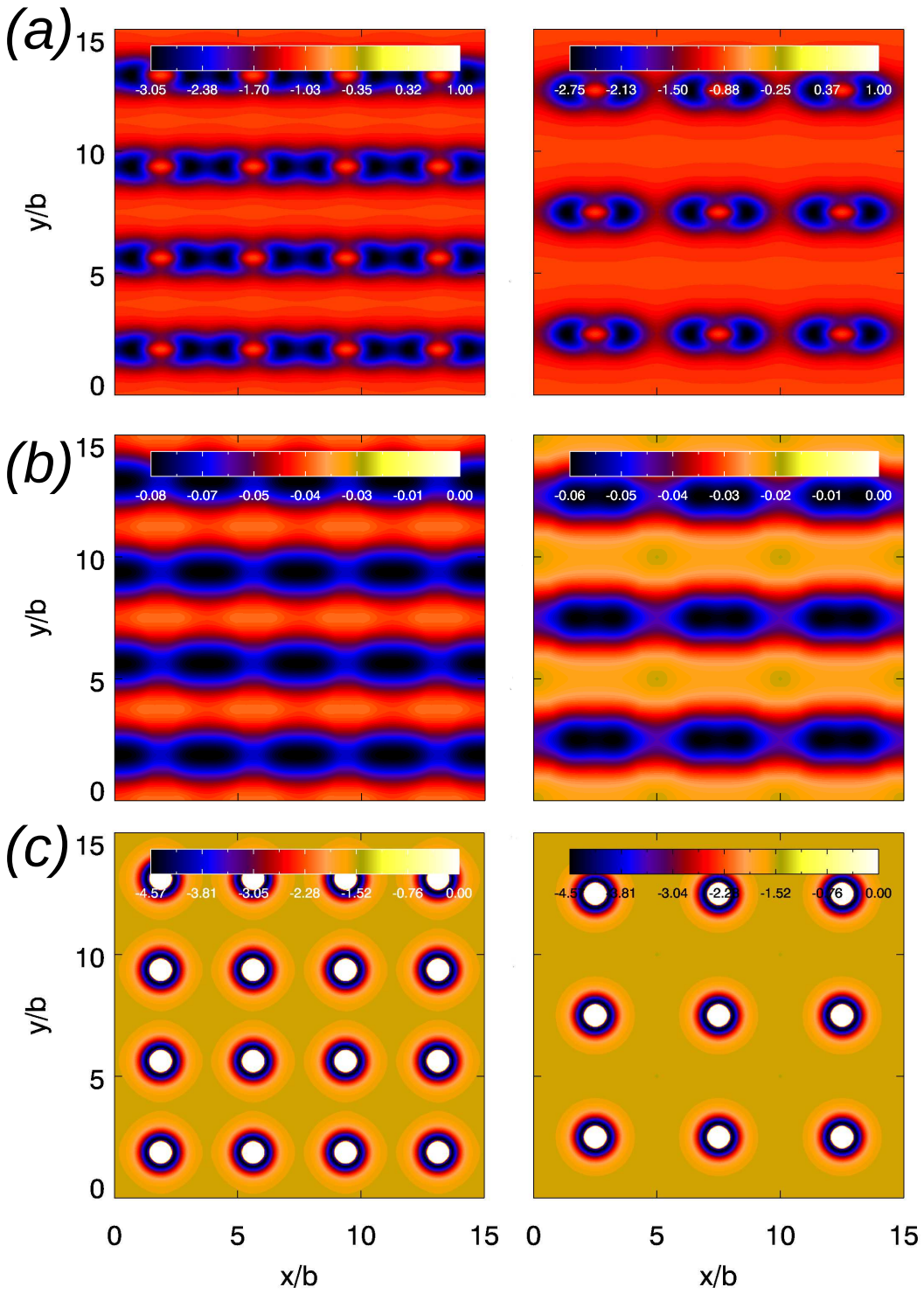

Fig. 2 D. L. Cheung

Journal of Chemical Physics

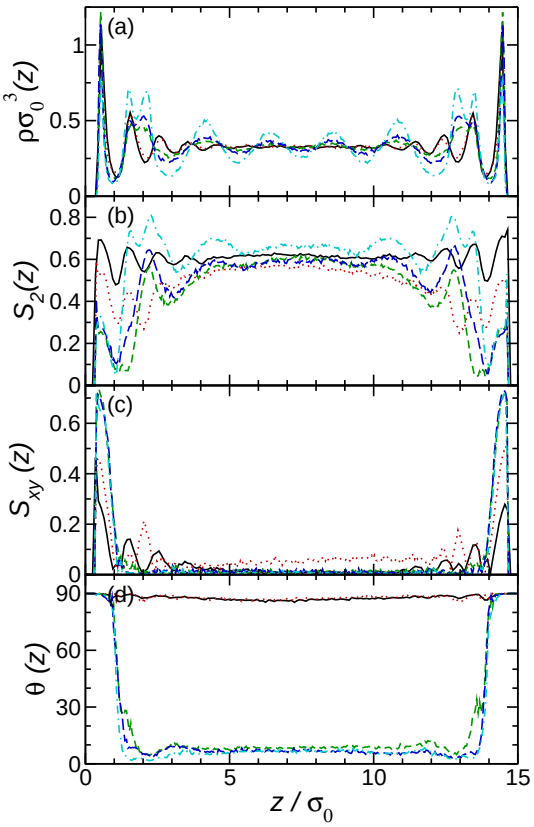

Fig. 3 D. L. Cheung

Journal of Chemical Physics

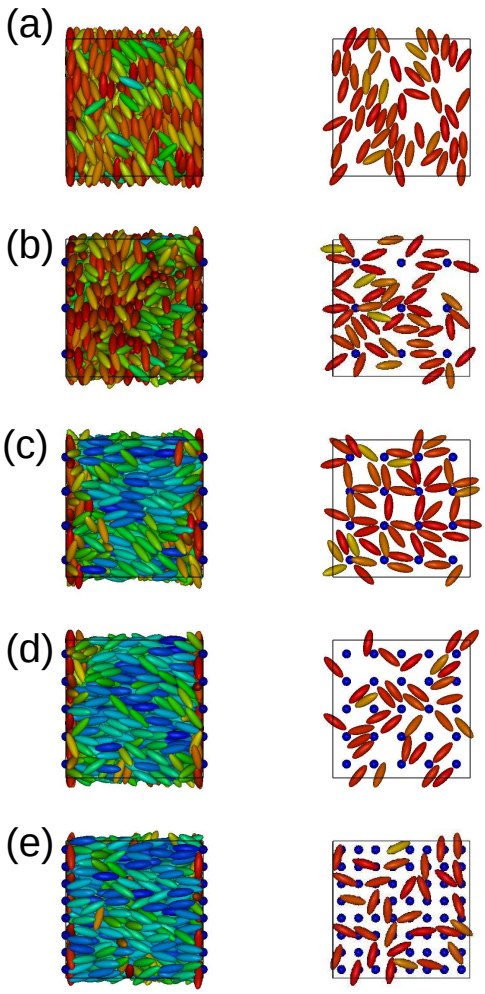

Fig. 4 D. L. Cheung

Journal of Chemical Physics

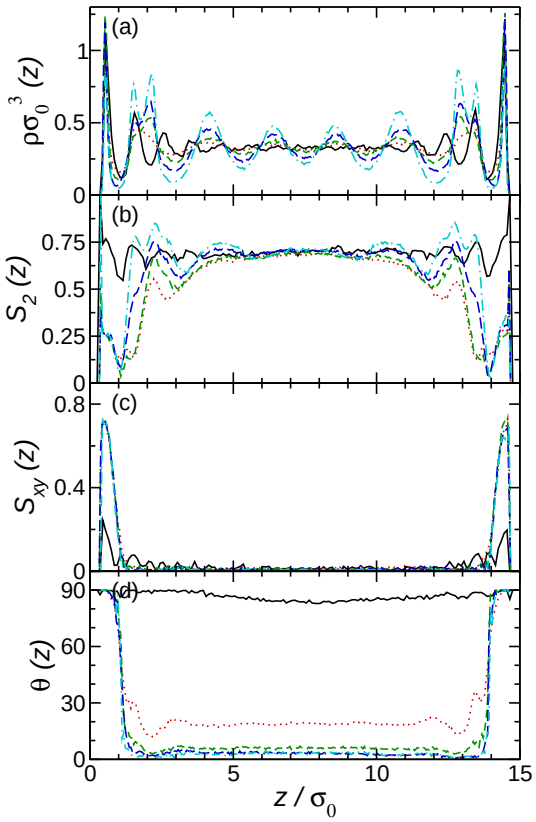

Fig. 5 D. L. Cheung

Journal of Chemical Physics

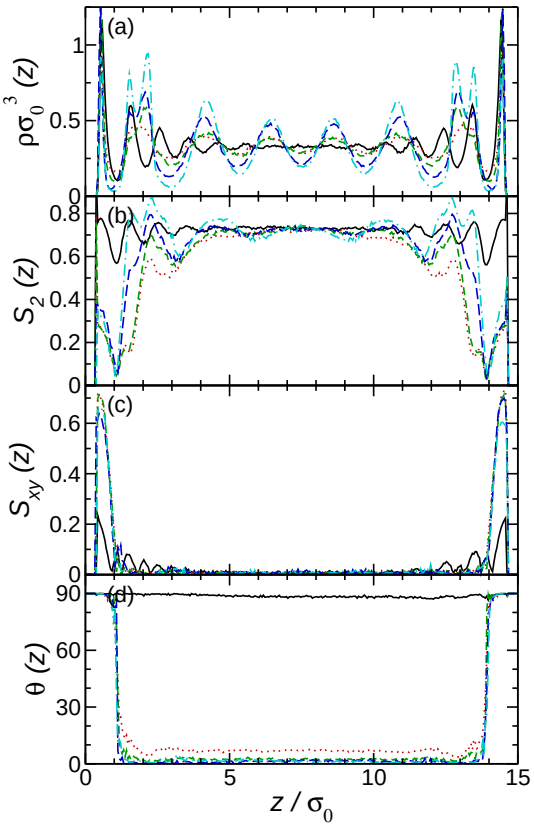

Fig. 6 D. L. Cheung

Journal of Chemical Physics